International Journal of Scientific Engineering and Applied Science (IJSEAS) – Volume-2, Issue-2, February 2016
ISSN: 2395-3470
www.ijseas.com

High Temperature and High Strain Rate Superplastic Deep Drawing Process for AA2618 Alloy Cylindrical Cups

Chennakesava R Alavala
Department of mechanical Engineering, JNT University, Hyderabad, India

Abstract

In this present work, the formability of high temperature and high strain rate deep drawing process were evaluated for the cylindrical cups using Taguchi technique and finite element analysis. The process parameters were temperature, strain rate, coefficient of friction and blank holder velocity. The formability limit diagrams were developed for all the trials. The AA2618 sheets were used for the deep drawing of the cylindrical cups. The formability of the cups was outstanding for the temperature of 500^{o}C and strain rate of 1.0 s^{-1}.

Keywords: *AA2618 alloy, high temperature, high strain rate, superplastic deep drawing process, coefficient of friction, forming limit diagram.*

1. Introduction

The deformation has been enhanced by several times during deep drawing without fracture at higher temperatures. The significance of high strain rate superplastic (HSRS) forming process is to reduce the forming time [1]. Numerous investigations have been carried out to enhance the superplastic properties of aluminum alloys. During cup drawing process, the influence of process parameters blank thickness, temperature, coefficient of friction and strain rate was investigated for 1050 [2], 1070 [3], 1080 [4], 1100 [5], 2014 [6], 2017 [7], 2024 [8], 2219 [9] and 5083 [10] aluminum alloys. The deep drawing process was also carried out for Al-Mg alloy [11], Ti-Al-4V alloy [12], EDD steel [13] and gas cylinder steel [14]. In the finite element simulations, a forming limit diagram (FLD) has been successfully applied to analyze the fracture phenomena by comparing the strain status [7, 8, 9].

The significance of the present work was to find fitness of AA2618 alloy for high temperature and high strain rate superplastic (HTHSR) forming process. The investigation was focused on the process parameters such as temperature, strain rate, coefficient of friction and blank holder velocity. The design of experiments was carried out using Taguchi technique. The HTHSR superplastic deep drawing process was executed using the finite element analysis software namely D-FORM 3D.

2. Material and Methodology

In the present work, AA2618 alloy was used to fabricate cylindrical cups. The levels chosen for the controllable process parameters are summarized in table 1. Each of the process parameters was studied at three levels. The orthogonal array (OA), L9 was selected to carry out experimental and finite element analysis (FEA). The assignment of parameters in the OA matrix is given in table 2.

Table 1: Control parameters and levels

Factor	Symbol	Level–1	Level–2	Level–3
Temperature, ^{0}C	A	300	400	500
Strain rate, 1/s	B	0.01	0.1	1
Coefficient of friction	C	0.10	0.15	0.20
BH velocity, mm/s	D	0.4	0.5	0.6

Table 2: Orthogonal array (L9) and control parameters

Treat No.	A	B	C	D
1	1	1	1	1
2	1	2	2	2
3	1	3	3	3
4	2	1	2	3
5	2	2	3	1
6	2	3	1	2
7	3	1	3	2
8	3	2	1	3
9	3	3	2	1

The finite element modeling and analysis was carried using D-FORM 3D software. The cylindrical sheet blank was created with desired diameter and thickness using CAD tools. The cylindrical top punch, cylindrical bottom hollow die were also modeled with appropriate inner and outer radius and corner radius using CAD tools. The clearance between the

punch and die was calculated as in Eq. (2). The sheet blank was meshed with tetrahedral elements.

Drawing force, $F_d = \pi dt[D/d - 0.6]\sigma_y$ (1)

Clearance, $c = t \pm \mu\sqrt{10t}$ (2)

In the present work, moving blank die was used to hold the blank at a predefined speed different to the punch speed. The contact between blank/punch and die/blank were coupled as contact pair (Fig. 1). The mechanical interaction between the contact surfaces was assumed to be frictional contact and modeled as Coulomb's friction model [15].

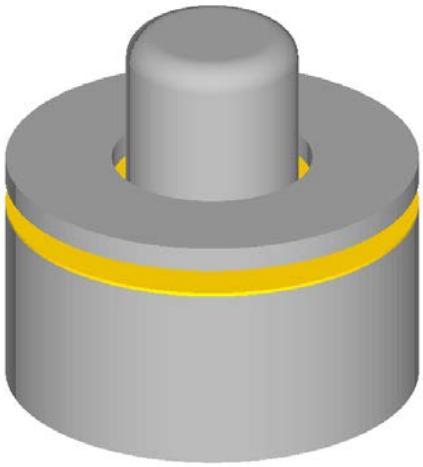

Fig.1 Cylindrical cup drawing with movable blank holder die.

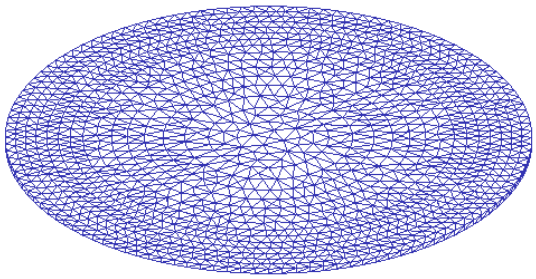

Fig.2 Discretization of 2618 Al-alloy blank.

3. Results and Discussion

The modeling parameters of deep drawing process were as follows:
Number of tetrahedron elements for the blank (Fig. 2): 8117
Number of polygons for top die: 9120
Number of polygons for bottom die: 9600
Number of polygons for moving blank die: 960

3.1 Influence of process parameters on effective stress

The percent contributions of A, B, C and D vary over a range between 17.45% and 32.44% towards the total variation in the effective stress (Table 3). The temperature (A) by itself has an effect of 17.45% on the effective stress. The coefficient of friction (B) can cause 24.84% of total variation in the effective stress. The strain rate (C) has contributed one-fourth (25.27%) of the total variation in the effective stress. The blank holder (BH) velocity (D) has given nearly one-third (32.44%) of the total variation in effective stress.

Table 3: ANOVA summary of the effective stress

Source	Sum 1	Sum 2	Sum 3	*SS*	*v*	*V*	*F*	*P*
A	1352.08	1265	1026	18954	1	18954	1958928	17.45
B	1049.02	1438	1156	26991	1	26991	2789633	24.84
C	981	1349	1313	27451	1	27451	2837176	25.27
D	1106	1479	1058.97	35247	1	35247	3642922	32.44
e				0.01	4	0.00	0.00	0.00
T	4488	5531	45543	108644	8			100

Note: *SS* is the sum of square, *v* is the degrees of freedom, *V* is the variance, *F* is the Fisher's ratio, *P* is the percentage of contribution and *T* is the sum squares due to total variation.

Fig. 3a presents the effective stress induced in AA2618 alloy during cup drawing process as a function of temperature. The effective stress was 225.35 MPa and 171.06 MPa at the lowest (300^{o}C) and highest (500^{o}C) operating temperatures, respectively; it was 210.80 MPa at temperature of 400^{o}C. The effective stress decreased with the increase of temperature. The same trend is clearly observed in all trials (Fig. 3b). Fig. 4 describes the effective stress as a function of strain rate. As per the planning of the Taguchi experimentation and optimization, the effective stress initially increases with the increase of the strain rate till it reaches a value of 0.1 s^{-1} and later on the effective stress decreases with the increases of strain rate from 0.1 to 1.0 s^{-1}. However, the strain rates were high as outputs from the finite element analysis. But, the trend was same. This reduction in stress took place when the

strain and strain rate hardening effects were outweighed by the softening effect as result of the heat generated during plastic deformation [16].

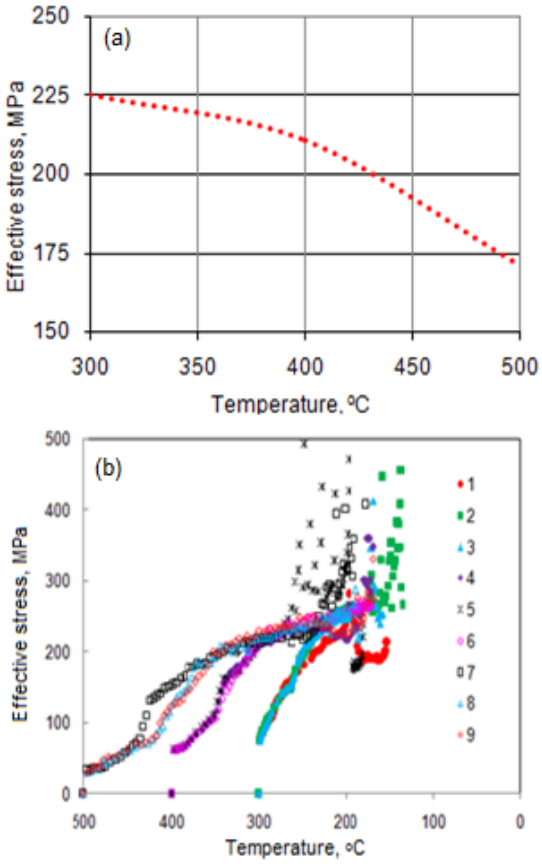

Fig. 3 Effect of temperature on the effective stress induced in all trials.

As the coefficient of friction varied from 0.1 to 0.15, the effective stress increased from 163.50 MPa to 224.82 MPa and its value was decreased above 0.2 value of coefficient of friction (Fig. 5). In deep drawing process, friction initiates from sliding contact between the tool and the blank sheet. Fig. 6 depicts the effective stress as a function of blank holder velocity. In the present work, the blank holder (BH) was allowed to move along with the punch but at different velocities. The effective stress was 184.28 MPa and 246.42 MPa at the lowest (0.4 mm/s) and highest (0.5 m/s) operating BH velocity; it was 184.00 MPa at BH velocity of 0.6 mm/s.

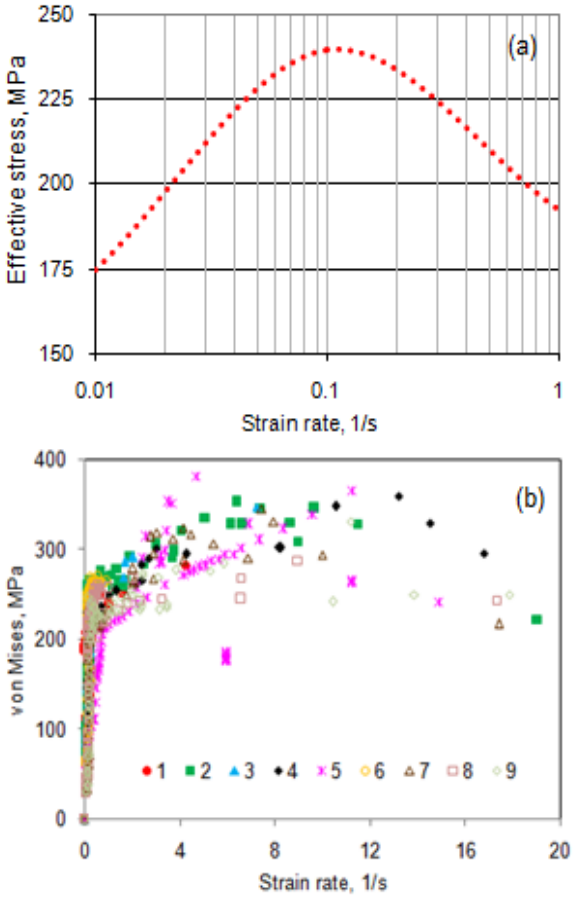

Fig. 4 Effect of strain rate on the effective stress induced in all trials.

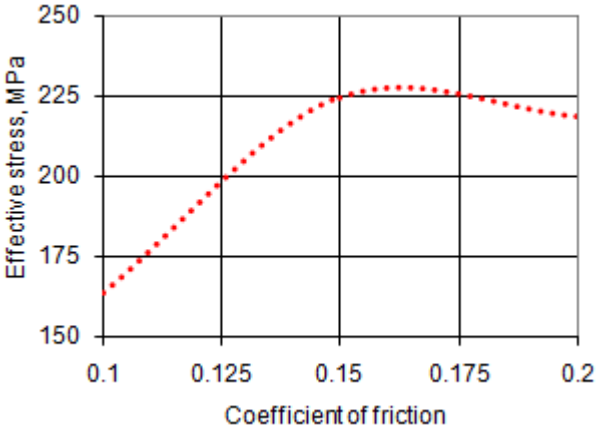

Fig. 5 Effect of friction coefficient on the effective stress.

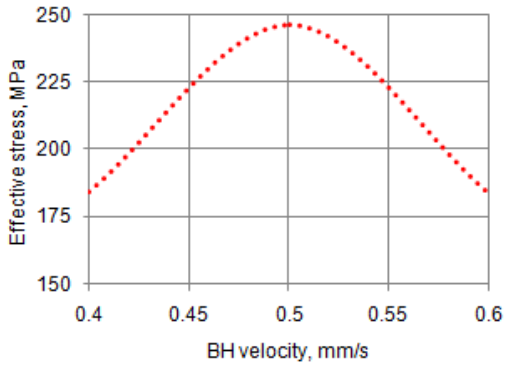

Fig. 6 Effect of friction coefficient on the effective stress.

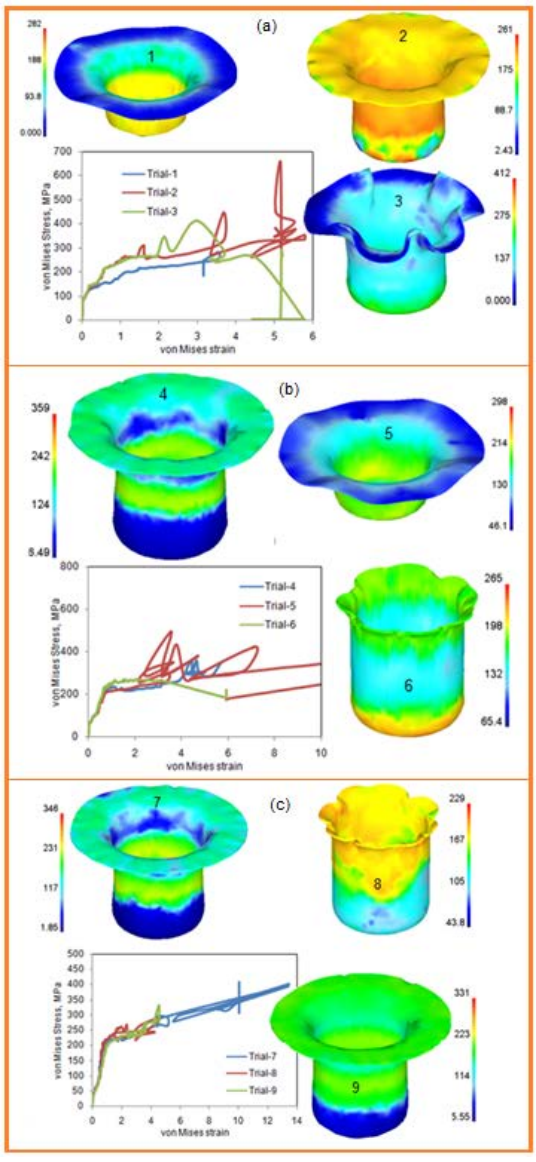

Fig. 7 Effect of process parameters on the effective stress.

The FEA results of effective stress are shown in Fig. 7 for various test conditions as per the design of experiments. For trials 1, 2 and 3, the temperature was 300°C and other process parameters were varied as mentioned in tables 1 and 2. The effective stresses for trails 1, 2 and 3 were, respectively, 282 MPa, 261 MPa and 412 MPa (Fig. 7a). For trials 4, 5 and 6, the temperature was 400°C and other process parameters were as stated in tables 1 and 2. The effective stresses for trails 4, 5 and 6 were, respectively, 359 MPa, 298 MPa and 265 MPa (Fig. 7b). For trials 7, 8 and 9, the temperature was 500°C and other process parameters were as designed in tables 1 and 2. The effective stresses for trails 7, 8 and 9 were, respectively, 346 MPa, 229 MPa and 331 MPa (Fig. 7c).

3.2 Influence of Process Parameters on Surface Expansion Ratio

In the deep drawing process the plastic deformation in the surface is much more pronounced than in the thickness. The ANOVA summary of surface expansion ratio is given in table 4. As per the Fisher's test (F = 3.01), the temperature, (A), coefficient of friction (B), strain rate (C) and BH velocity (D) could contribute, respectively, 22.94%, 31.91%, 22.79% and 22.36% respectively towards the total variation in the surface expansion ratio.

Table 4: ANOVA summary of the surface expansion ratio

Source	Sum 1	Sum 2	Sum 3	*SS*	*v*	*V*	*F*	*P*
A	29.07	180.41	1150.3	246745	1	246745	9989677	22.94
B	1281.73	46.39	31.65	343220	1	343220	13895556	31.91
C	8.13	207.7	1143.9	245159	1	245159.8	9925496	22.79
D	52.03	1143.8	163.93	240519	1	240519	9737607	22.36
e				0.0247	4	0.01	0.40	0
T	1370.96	1578.3	2489.8	1075643	8			100

The surface expansion ratio would increase with an increase in the operating temperature from 300°C to 500°C (Fig. 8). The effect of strain rate on the surface expansion ratio is shown in Fig. 9. The surface expansion ratio decreased with increase in the strain rate. The surface expansion ratio was increased with the increasing the coefficient of friction (Fig. 10). The surface expansion ratio was high for the blank holder velocity of 0.5 m/s (Fig. 11). At high velocities, the blank holder would come in contact with the blank early and accordingly, the material

was restrained to flow into the die resulting reduction in the surface expansion.

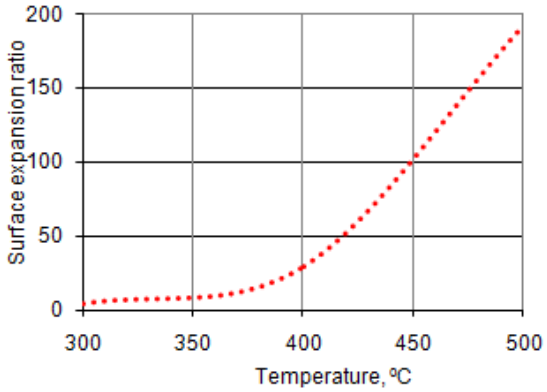

Fig. 8 Effect of temperature on the surface expansion ratio.

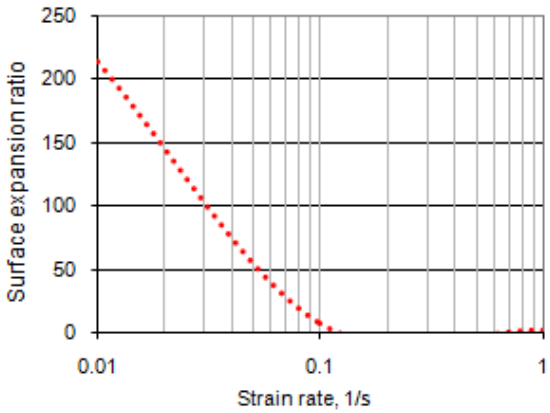

Fig. 9 Effect of strain rate on the surface expansion ratio.

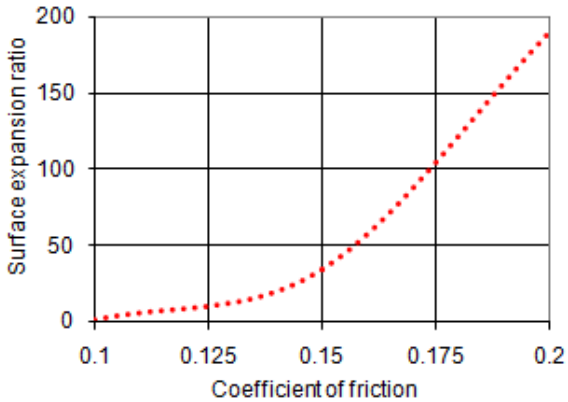

Fig.10 Effect of friction coefficient on the surface expansion ratio.

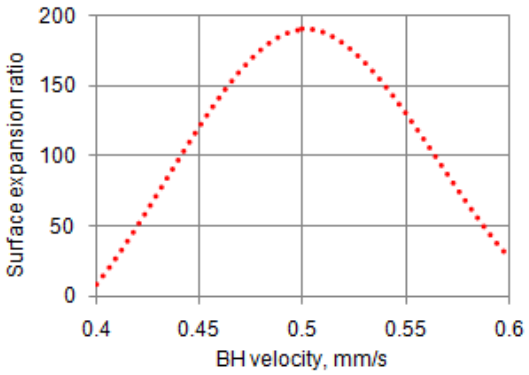

Fig. 11 Effect of BH velocity on the surface expansion ratio.

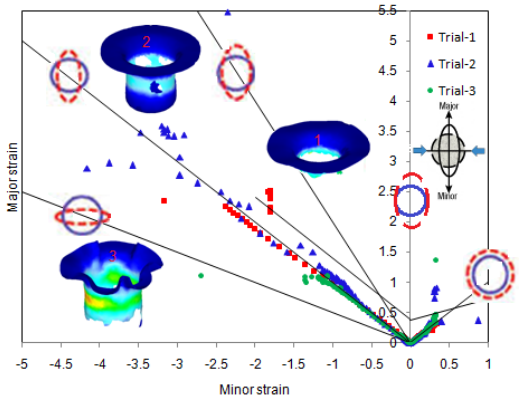

Fig. 12 Forming limit diagram with damage in the cups drawn at temperature 300°C.

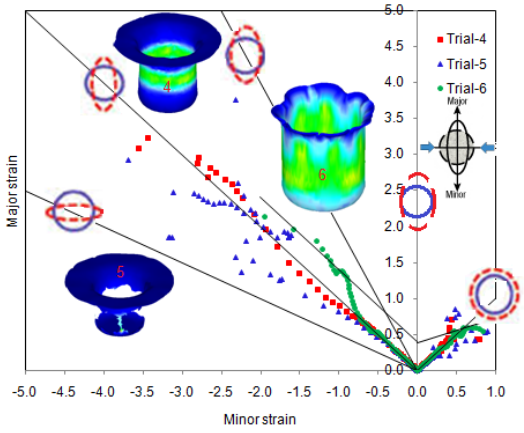

Fig. 13 Forming limit diagram with damage in the cups drawn at temperature 400°C.

3.3 Forming limit diagrams and damages in the cups

Fig. 12 depicts the forming limit diagram (FLD) with damages in the cylindrical cups drawn from AA2618 sheets at temperature 300°C. The FLD for the

cylindrical cup drawn under trial 1 was ruptured because of pure tension and shear. The fracture has occurred in the cups drawn with trial 2 due to shear. For cups drawn with trial 3, the fracture was due to biaxial tension and compression. Fig. 13 illustrates the forming limit diagram and damages in the cups drawn from AA2618 sheets with trials, 4, 5 and 6 at temperature 400°C. Cups drawn on trial 4 were undergone deep drawing process with strain rate of 158 s^{-1}. Cups drawn from trials 5 were fractured due to shear and compression. No fracture was observed in the cups drawn with trail 6. Cups drawn from trial 7 were experienced high deep drawing process with strain rate of 1120 s^{-1}. Cups drawn under trial 8 were fractured in the flange region due to shear and stretching (Fig. 14). Cups drawn under trial 9 did not have any fracture. Cups drawn from trials 8 were fractured due to shear and compression. The damage factor was high (17.14) with trial 2 (Fig. 15) while it was 0.98 for trail 6.

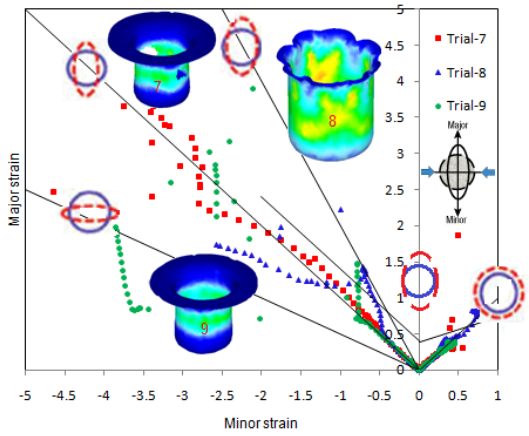

Fig.14 Forming limit diagram with damage in the cups drawn at temperature 500°C.

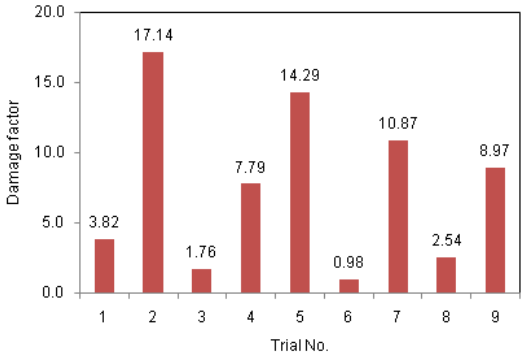

Fig.15 Damage factors under different trials.

4. Conclusion

The effective stress decreases with the increase of temperature. The optimum strain rate was 0.1 s^{-1}. AA2618 has been found to yield successful cups at high temperature and high strain rate.

Acknowledgment

The author wishes to thank University Grants Commission (UGC), New Delhi, India for financial assisting this project.

References

1. R. L. Hecht and K. Kannan, in: A.K. Gosh, T.R. Bieler (Eds.), "Superplasticity and Superplastic Forming," TMS, Warrendale, PA, USA, 1995, p. 259, 1995.
2. A. C. Reddy, "Homogenization and Parametric Consequence of Warm Deep Drawing Process for 1050A Aluminum Alloy: Validation through FEA," International Journal of Science and Research, Vol. 4, No. 4, 2015, pp. 2034-2042.
3. K. Chandini and A. C. Reddy, "Parametric Importance of Warm Deep Drawing Process for 1070A Aluminium Alloy: Validation through FEA," International Journal of Scientific & Engineering Research, Vol. 6, No. 4, 2015, pp. 399-407.
4. B. Yamuna and A. C. Reddy, "Parametric Merit of Warm Deep Drawing Process for 1080A Aluminium Alloy: Validation through FEA," International Journal of Scientific & Engineering Research, Vol. 6, No. 4, 2015, pp. 416-424.
5. T. Srinivas and A. C. Reddy, "Parametric Optimization of Warm Deep Drawing Process of 1100 Aluminum Alloy: Validation through FEA," International Journal of Scientific & Engineering Research, Vol. 6, No. 4, 2015, pp. 425-433.
6. A. C. Reddy, "Parametric Optimization of Warm Deep Drawing Process of 2014T6 Aluminum Alloy Using FEA," International Journal of Scientific & Engineering Research, Vol. 6, No. 5, 2015, pp. 1016-1024.
7. A. C. Reddy, "Finite Element Analysis of Warm Deep Drawing Process for 2017T4 Aluminum Alloy: Parametric Significance Using Taguchi Technique," International Journal of Advanced Research, Vol. 3, No. 5, 2015, pp. 1247-1255.
8. A. C. Reddy, "Parametric Significance of Warm Drawing Process for 2024T4 Aluminum Alloy through FEA," International Journal of Science and Research, Vol. 4, No. 5, 2015, pp. 2345-2351.
9. A. C. Reddy, "Formability of High Temperature and High Strain Rate Superplastic Deep Drawing Process

for AA2219 Cylindrical Cups," International Journal of Advanced Research, Vol. 3, No. 10, 2015, pp. 1016-1024.

10. S.N. Patankar and T.M. Jen, "Strain Rate Insensitive Plasticity in Aluminum Alloy 5083," Scripta Materialia, Vol. 38, 1998, pp.1255-1261.
11. F. Shehata, M. J. Painter and R. Pearce, "Warm forming of aluminum/magnesium alloy sheet, Journal of Mechanics," Working Technology, Vol. 2, , 1978, pp.279-291.
12. A. C. Reddy, "Finite element analysis of reverse superplastic blow forming of Ti-Al-4V alloy for optimized control of thickness variation using ABAQUS," Journal of Manufacturing Engineering, Vol.01, No.01, 2006, pp.06-09.
13. A. C. Reddy, T. K. K. Reddy and M. Vidya Sagar, "Experimental characterization of warm deep drawing process for EDD steel," International Journal of Multidisciplinary Research & Advances in Engineering, ISSN: 0975-7074, Vol. 04, No. 03, 2012, pp.53-62.
14. A. C. Reddy, "Evaluation of local thinning during cup drawing of gas cylinder steel using isotropic criteria," International Journal of Engineering and Materials Sciences, Vol.5, No.2, 2012, pp.71-76.
15. C.R. Alavala, Finite Element Methods: Basic Concepts and Applications, New Delhi, PHI Learning Pvt. Ltd: 2008.
16. L. Clarisse, A. Bataille, Y. Pennec, J. Crampon and R. Duclos, "Investigation of grain boundary sliding during superplastic deformation of a fine-grained alumina by atomic force microscopy," Ceramics International, Vol. 25, 1999, pp. 389-394.